Correspondence between Layer Morphology and Intralayer Excitation Transport Dynamics in Zirconium−Phosphonate Monolayers

J. C. Horne,[†] Y. Huang,[‡] G.-Y. Liu,[‡] and G. J. Blanchard*[,†]

Contribution from the Departments of Chemistry, Michigan State University, East Lansing, Michigan 48824-1322, and Wayne State University, Detroit, Michigan 48202

Received June 22, 1998

Abstract: We use atomic force microscopy (AFM) in conjunction with fluorescence relaxation dynamics to establish the relationship between the physical morphology and optical response of zirconium−phosphonate (ZP) monolayers containing oligothiophene chromophores. For ZP monolayers formed on SiO_x, island structures are seen with AFM in the size range 40−100 Å with the nearest neighbor island spacing varying from 80 to 200 Å. For these same surfaces, the fluorescence population relaxation dynamics we measure are nonexponential, chromophore concentration-independent, and identical for two different chromophores. This finding is fully consistent with the AFM data, and the results can be understood using an excitation hopping model. The spectroscopic data are consistent with aggregated islands ∼50−100 Å in diameter. We demonstrate that the spectroscopic and physical domain sizes present on ZP/SiO_x monolayers are the same. Studies using several initial priming schemes point to the silanol group distribution on the surface determining structural heterogeneity with intermolecular interactions between chromophores playing a secondary role.

Introduction

Achieving predictive control over surface properties has become a substantial effort in interfacial chemistry and materials science research. The ability to achieve this level of control has been determined to a large extent by the propensity of certain types of molecules to self-assemble at various metallic and dielectric interfaces. Alkanethiol self-assembly onto gold is perhaps the most widely studied example of this process,[1−3] and there has been a great deal learned about the chemical modification of surfaces from this body of work. The ultimate utility of gold-thiol chemistry is limited both by the long-term robustness of the monolayer[4,5] and by the fact that there is not yet a general route to forming more complex, multilayer structures with this system. Chemistry that allows the controlled, sequential assembly of multiple layers creates possibilities for a much broader array of chemical and physical phenomena to be explored. Both silane chemistry[6−8] and metal−phosphonate (MP) chemistry[9−25] have been developed for this purpose. MP multilayer chemistry has proven to be particularly useful and has been explored for its use in potential applications such as artificial photosynthesis, light harvesting, and optical information storage.[11,19,20,26−28] The complexes formed between phosphonates and several metal ions are very insoluble, allowing for the facile buildup of individual layers with robust interlayer connections. The resulting three-dimensional structural integrity stands in sharp contrast to Langmuir−Blodgett multilayer structures.

Key to the utility of MP systems for many applications is the morphology of the layer(s) they form. This is especially true when the optical properties of the monolayer are the subject of investigation because mesoscopic structural features in the

[†] Michigan State University.
[‡] Wayne State University.
* Author to whom correspondence should be addressed.

(1) Ulman, A. *Chem. Rev.* **1996**, *96*, 1533.
(2) Dubois, L. H.; Nuzzo, R. G. *Annu. Rev. Phys. Chem.* **1992**, *43*, 437.
(3) Xia, Y.; Whitesides, G. M. *Angew. Chem., Int. Ed. Engl.* **1998**, *37*, 551.
(4) Karpovich, D. S.; Blanchard, G. J. *Langmuir* **1994**, *10*, 3315.
(5) Schessler, H. M.; Karpovich, D. S.; Blanchard, G. J. *J. Am. Chem. Soc.* **1996**, *118*, 9645.
(6) Gun, J.; Iscovici, R.; Sagiv, J. *J. Colloid Interface Sci* **1984**, *101*, 201.
(7) Maoz, R.; Sagiv, J. *J. Colloid Interface Sci.* **1984**, *100*, 465.
(8) Maoz, R.; Sagiv, J. *Thin Solid Films* **1985**, *132*, 135.
(9) Hong, H.-G.; Sackett, D. D.; Mallouk, T. E. *Chem. Mater.* **1991**, *3*, 521.
(10) Thompson, M. E. *Chem. Mater.* **1994**, *6*, 1168.
(11) Katz, H. E.; Wilson, W. L.; Scheller, G. *J. Am. Chem. Soc.* **1994**, *116*, 6636.
(12) Yonemoto, E. H.; Saupe, G. B.; Schmehl, R. H.; Hubig, S. M.; Riley, R. L.; Iverson, B. L.; Mallouk, T. E. *J. Am. Chem. Soc.* **1994**, *116*, 4786.
(13) Katz, H. E.; Bent, S. F.; Wilson, W. L.; Schilling, M. L.; Ungashe, S. B. *J. Am. Chem. Soc.* **1994**, *116*, 6631.
(14) Frey, B. L.; Hanken, D. G.; Corn, R. M. *Langmuir* **1993**, *9*, 1815.
(15) Yang, H. C.; Aoki, K.; Hong, H.-G.; Sackett, D. D.; Arendt, M. F.; Yau, S.-L.; Bell, C. M.; Mallouk, T. E. *J. Am. Chem. Soc.* **1993**, *115*, 11855.
(16) Vermeulen, L.; Thompson, M. E. *Nature* **1992**, *358*, 656.
(17) Ungashe, S. B.; Wilson, W. L.; Katz, H. E.; Scheller, G. R.; Putvinski, T. M. *J. Am. Chem. Soc.* **1992**, *114*, 8717.
(18) Cao, G.; Rabenberg, L. K.; Nunn, C. M.; Mallouk, T. M. *Chem. Mater.* **1991**, *3*, 149.
(19) Katz, H. E.; Schilling, M. L.; Chidsey, C. E. D.; Putvinski, T. M.; Hutton, R. S. *Chem. Mater.* **1991**, *3*, 699.
(20) Katz, H. E.; Scheller, G.; Putvinski, T. M.; Schilling, M. L.; Wilson, W. L.; Chidsey, C. E. D. *Science* **1991**, *254*, 1485.
(21) Putvinski, T. M.; Schilling, M. L.; Katz, H. E.; Chidsey, C. E. D.; Mujsce, A. M.; Emerson, A. B. *Langmuir* **1990**, *6*, 1567.
(22) Rong, D.; Hong, H.-G.; Kim, Y.-I.; Krueger, J. S.; Mayer, J. E.; Mallouk, T. E. *Coord. Chem. Rev.* **1990**, *97*, 237.
(23) Lee, H.; Kepley, L. J.; Hong, H.-G.; Akhter, S.; Mallouk, T. E. *J. Phys. Chem.* **1988**, *92*, 2597.
(24) Lee, H.; Kepley, L. J.; Hong, H.-G.; Mallouk, T. E. *J. Am. Chem. Soc.* **1988**, *110*, 618.
(25) Katz, H. E. *Chem. Mater.* **1994**, *6*, 2227.
(26) Vermeulen, L. A.; Snover, J. L.; Sapochak, L. S.; Thompson, M. E. *J. Am. Chem. Soc.* **1993**, *115*, 11767.
(27) Snover, J. L.; Byrd, H.; Suponeva, E. P.; Vicenzi, E.; Thompson, M. E. *Chem. Mater.* **1996**, *8*, 1490.
(28) Kaschak, D. M.; Mallouk, T. E. *J. Am. Chem. Soc.* **1996**, *118*, 4222.

10.1021/ja982182r CCC: $18.00
Published on Web 04/27/1999

Scheme 1. Structures of Bis(phosphonates) Used in This Work: (a) the Donor, 2,2′-Bithiophene-5,5′-diyl-bis(phosphonic acid) (BDP), (b) the Acceptor, 2,2′:5′,2″:5″,2‴-Quaterthiophene-5,5‴-diylbis(phosphonic acid) (QDP), and (c) the Diluent, 1,12-Dodecanediyl-bis(phosphonic acid) (DDBPA)

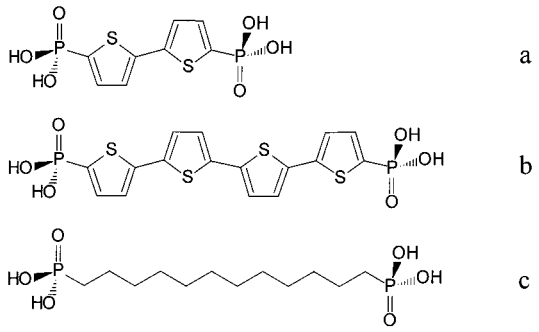

monolayer can and do mediate the optical response and relaxation dynamics of chromophores within the layer. We are concerned with the relationship between physical morphology and optical response because of the potential utility of MP materials for optical information storage applications. Specifically, the efficiency of intralayer and interlayer excitation transport will depend sensitively on the mesoscopic structural features of the monolayers.

In this paper, we focus on elucidating the relationship between mesoscopic physical features seen with AFM measurements and molecular-scale excitation transport behavior of chromophores in the same monolayer assemblies. We use bisphosphonated oligothiophene chromophores because of their structural rigidity and spectroscopic properties. Isomerization about the inter-ring bond in oligothiophenes is facile in both the S_0 and S_1 states,[29] and this process does not complicate the structural or spectroscopic properties of the monolayers. To make rigid monolayer structures with favorable optical properties, we use 2,2′-bithiophene-5,5′-diylbis(phosphonic acid) (BDP) as the photon donating chromophore and 2,2′:5′,2″:5″,2‴-quaterthiophene-5,5‴-diylbis(phosphonic acid) (QDP) for the photon acceptor chromophore. The structures of these molecules are shown in Scheme I.

Atomic force microscopy (AFM) images of our zirconium−phosphonate (ZP) monolayers reveal the existence of islands with a characteristic size in the range 40−100 Å. The nearest neighbor spacing of these islands varies from 80 to 200 Å. We have made a series of monolayers with varying donor and acceptor chromophore concentrations, and for all of these monolayers, we recover the same nonexponential population decay. We use the transient fluorescence data to recover spectroscopic domain sizes for the aggregates 50−100 Å in diameter using an excitation transport model used previously for stilbazolium dyes in Langmuir−Blodgett films.[30] The agreement between the physical (AFM) and spectroscopic measurements of the surface morphology is remarkable, and this finding implies a significant degree of intermolecular alignment within the individual aggregate domains. The invariance of the optical response of these monolayers as a function of changes in the initial priming chemistry of the SiO_x substrate indicates that the surface silanol group distribution mediates the observed structural heterogeneity of the monolayers.

Experimental Section

Metal−Phosphonate Monolayer Synthesis. Polished silicon (100) substrates (MultiCrystal Optics or Boston Piezo-Optics) were cleaned by immersion in piranha solution *(Caution: Piranha solution is extremely corrosive and is a potent oxidizer!)* for 10 min and rinsed with flowing distilled water, followed by hydrolysis in 2 M HCl for 5 min and a final distilled water rinse. Samples were dried with a N_2 stream and were primed immediately. The substrates were primed with (3-aminopropyl)triethoxysilane (APTES) or (3-aminopropyl)dimethylethoxysilane (APDMES). Substrates were refluxed in a 1% v/v solution of APTES in anhydrous octane for 10 min, followed by rinses in hexane and water. Alternatively, they were immersed in a 0.5% v/v solution of APDMES in anhydrous toluene overnight and rinsed with methanol and water. After drying with N_2, the aminated surface was derivatized to the phosphonate using a solution of 0.2 M $POCl_3$ and 0.2 M collidine in anhydrous CH_3CN for 20 min, followed by rinses with CH_3CN and water. The resulting surface was exposed to Zr^{4+} by immersion in a 5 mM solution of $ZrOCl_2$ in 60% aqueous ethanol for 10 min. The syntheses of 2,2′-bithiophene-5,5′-diylbis(phosphonic acid) (BDP) and 2,2′:5′,2″:5‴;2‴-quaterthiophene-5,5‴-diylbis(phosphonic acid) (QDP) and 1,12-dodecanebis(phosphonic acid) (DDBPA) have been reported previously,[19,31] and we show their structures in Scheme 1. We synthesized monolayers from 1 mM bis(phosphonate) solutions where the donor BDP is 5% of the total bis(phosphonate) concentration (0.05 mM) and varying amounts of acceptor QDP (1−95%, 0.01−0.95 mM) are used. The remainder of the monolayer is comprised of an optically inactive component, DDBPA, which, in its all-trans conformation, is approximately the same length as the all-anti conformation of the acceptor QDP. There is no requirement, a priori, that the fractional composition of the monolayers should be the same as that of the solutions from which they are made. We have investigated this matter extensively and have found experimental conditions where there is a direct correspondence and cases where there is not. For example, deposition of BDP and 1,6-hexanediylbis(phosphonic acid) (HBPA) from ethanol produces a monolayer where BDP is adsorbed preferentially to the surface.[31] Conversely, the deposition of QDP from a solution of 80% DMSO, 18% EtOH, and 2% H_2O yields a monolayer where the composition is related directly to the solution composition.[41] We find that this solvent system works equally well for both QDP and BDP.

Atomic Force Microscopy. The atomic force microscope utilized an in-house-constructed, deflection-type scanning head that exhibits high mechanical stability.[32] The scanner was controlled by an AFM100 preamplifier and STM1000 electronics manufactured by RHK Technology. Unless specified otherwise, all the images shown here were acquired with the sample covered with 2-butanol and using sharpened Si_3N_4 microlevers (Park Scientific Instruments) with a force constant of 0.1 N/m. Because imaging under liquids eliminates the capillary

(29) Horne, J. C.; Blanchard, G. J.; LeGoff, E. *J. Am. Chem. Soc.* **1995**, *117*, 9551.
(30) Song, Q.; Bohn, P. W.; Blanchard, G. J. *J. Phys. Chem. B* **1997**, *101*, 8865.
(31) Horne, J. C.; Blanchard, G. J. *J. Am. Chem. Soc.* **1996**, *118*, 12788.
(32) Xu, S.; Cruchon-Dupeyrat, S. J. N.; Garno, J. C.; Liu, G.-Y.; Jennings, G. K.; Yong, T. H.; Laibinis, P. E. *J. Chem. Phys.* **1998**, *108*, 5002.
(33) (a) Ohnesorge, F.; Binnig, G. *Science* **1994**, *260*, 1451. (b) Marti, O.; Drake, B.; Hansma, P. K. *Appl. Phys. Lett.* **1987**, *51*, 484. (c) Butt, H. J.; Seifert, K.; Bamberg, E. *J. Phys. Chem.* ***1993***, 97, 7316
(34) DeWitt, L.; Blanchard, G. J.; LeGoff, E.; Benz, M. E.; Liao, J. H.; Kanatzidis, M. G. *J. Am. Chem. Soc.* **1993**, *115*, 12158.
(35) (a)Chidsey, C. E. D.; Liu, G. Y.; Rowntree, P.; Scoles, G. *J. Chem. Phys.* **1989**, *91(7)*, 4421. (b) Poirier, G. E. *Langmuir* **199**4, 13, 2019. (c) McDermott, C. A.; McDermott, M. T.; Green, J. B.; Porter, M. D. *J. Phys. Chem.* **1995**, *99*, 13257. (d) Liu, G. Y., Xu, S., Cruchon-Dupeyrat, S. In *Thin Film: Self-Assembled Monolayers of Thiols*; Ulman, A., Ed.; Academic Press: 1998, Vol. 24, p 81.
(36) Förster, T. *Z. Naturforsch* **1949**, *A4*, 321.
(37) Förster, T. *Faraday Discuss. Chem. Soc.* **1959**, *27*, 7.
(38) Girard, C.; Martin, O. J. F.; Dereux, A. *Phys. Rev. Lett.* **1995**, *75*, 3098.
(39) Drexhage, K. H. *J. Lumin.* **1970**, *1, 2*, 693.
(40) The estimate of $R_0 = 57$ Å is based on an extinction coefficient of $\epsilon_{max} = 2.0 \times 10^7$ cm^2/mol for QDP, a fluorescence quantum yield of $\phi_{fl} = 0.9$ for BDP in solution and complete spectral overlap between the BDP emission spectrum and the QDP absorption spectrum.
(41) Horne, J. C.; Blanchard, G. J. *J. Am. Chem. Soc.* **1998**, *120*, 6336.

interaction between the AFM tip and the sample surface, imaging forces as low as 0.01−1 nN were used in order to yield higher resolution images than could be obtained in air.[33]

Lifetime Measurements. Time-correlated single photon counting spectroscopy (TCSPC) was used to measure the fluorescence lifetimes of the chromophores within the monolayers. This system has been described previously,[34] and we recap its salient features here. Short light pulses (∼5 ps fwhm) are generated with a cavity-dumped, synchronously pumped dye laser (Coherent 702-2) pumped by the second harmonic of the output of a mode-locked CW Nd:YAG laser (Quantronix 416). The dye laser output is frequency doubled ($LiIO_3$, Type I SHG) to excite the samples at 315 nm (630 nm fundamental, Kiton Red, Exciton). Monolayer samples were held approximately horizontally, with 5° tilts away from the horizontal in two directions; toward the excitation beam and toward the detector. Fluorescence from the sample was imaged through a reflecting microscope objective and collected across the emission bands of the chromophores with 30 nm fwhm detection bandwidth. The chromophore lifetimes we report here were fit to the sum of two exponential decays using commercial software (Microcal Origin v. 5.0) and are reported as the average of the fits of three decays and the associated standard deviations.

Steady-State Optical Spectroscopy. The absorbance spectra of oligothiophene chromophores in solution were measured using a Hitachi U-4001 UV−visible spectrophotometer. Spectra were collected with 5 nm resolution. Fluorescence spectra for solutions were measured on a Hitachi F-4500 fluorescence spectrometer. Excitation and emission slits were adjusted according to spectral intensity. Our previous reports on the linear response of oligothiophene monolayers have shown that their steady-state spectra are very similar to solution phase spectra,[31,41] and this similarity is demonstrated in Figure 1a,b for BDP.

Optical Null Ellipsometry. The thicknesses of primed substrates and monolayer samples were determined using a commercial optical null ellipsometer (Rudolph Auto-El II) operating at 632.8 nm. Data were acquired and reduced using Rudolph software. For both primer and ZP layers, we used a value of the refractive index of $\mathbf{n} = 1.462 + 0i$ for the determination of film thickness.

Results and Discussion

The focus of this work is on understanding the relationship between physical morphology and the optical response of layer constituents within a ZP monolayer. There is a substantial body of literature that demonstrates that ZP surfaces are not smooth, at least for the first several layers, and in such systems, it is important to devise means to understand any characteristic mesoscopic organization. We have used AFM measurements to elucidate the presence of island structures in ZP monolayers formed on oxidized Si or SiO_x. Because we are interested in these interfaces for potential optical information storage applications, it is critical that we understand the relationship between the physical morphology and optical response of the layers. Monolayers made with varying concentrations of oligothiophene chromophores exhibit the same island structures. These layers exhibit chromophore population decay dynamics that can be understood in the context of an excitation hopping model. From this model we can extract the size of the islands sensed spectroscopically and compare this information to the physical dimensions we recover from AFM measurements. The correspondence between the two measures of island size reflects the extent of intermolecular organization within the aggregates. AFM provides a physical image of surface topography with high resolution. The information derived spectroscopically gives molecular-scale insight into ordering within the islands. We consider the two bodies of information individually before discussing their correspondence.

Atomic Force Microscopy Measurements. We have imaged and compared the surfaces of oxidized silicon substrates, APTES-primed substrates, QDP monolayers on the primed substrates, and monolayers of 5% BDP, 50% QDP, and 45% DDBPA on the primed substrates. Example topographic images are shown in Figure 2. We found previously that the morphological differences between oxidized silicon and silica substrates mediate the motional freedom of the chromophores in the monolayer while population dynamics are not affected measurably by the substrate identity.[41] As shown in Figure 2a, the blank substrate is characterized by grooves in the oxidized surface that are 10−50 Å deep and ∼500 Å apart. The origin of these features is most likely mechanical polishing. Priming alters this morphology substantially. The grooves fill in and islands begin to appear when the substrate is reacted with APTES (Figure 2b). The overall surface roughness, 15−30 Å as determined by the fwhm of a histogram of the topographic images, is very similar for all four types of samples examined. The primer layer has a very distinct surface morphology, in which three-dimensional clusters with lateral dimension 20−200 Å are clearly visible. A typical nearest neighbor distance between clusters is ∼100 Å, although the separation between clusters varies from 50 to 1000 Å. Higher resolution images (e.g., 100 × 100 Å) taken at various locations on the surface reveal no long-range order or periodicity within an island. Thus the mesoscopic island structure originates from the nature of the initial priming layer chemistry. In contrast to thiol monolayers on gold,[35] we observe no crystalline ordering or structural regularity in these monolayers over length scales of more than a few molecules. We believe that the primer layer island formation is determined by primer polymerization in concert with a nonuniform silanol site distribution for these substrates.

The adsorption of QDP onto a primed and zirconated substrate results in a surface morphology similar to that seen for the primer layer (Figure 2c). Despite their outward similarity, there are some subtle differences between the primed and QDP-coated surfaces. Specifically, the QDP-terminated surface has a broader distribution in terms of aggregate lateral dimension and a

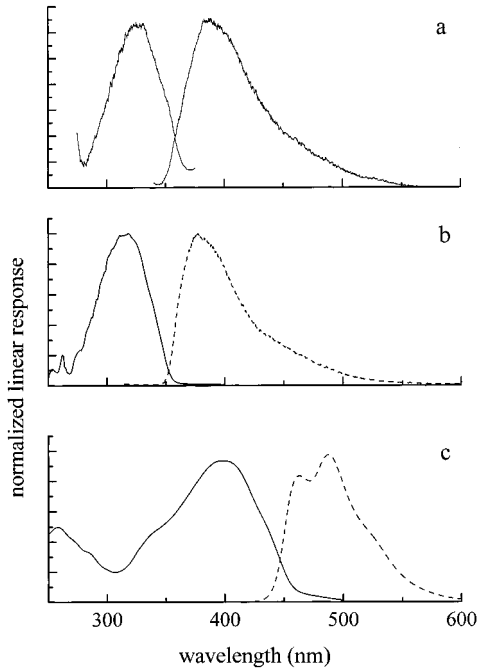

Figure 1. (a) Excitation and emission spectra for a 10% monolayer of BDP. For the excitation spectrum, the fixed emission monitoring wavelength was 400 nm, and for the emission spectrum, the excitation wavelength was 318 nm. (b) Absorption (—) and emission (- - -) spectra of 10^{-5} M BDP in DMSO. (c) Absorption (—) and emission (- - -) spectra of 10^{-5} M QDP in DMSO.

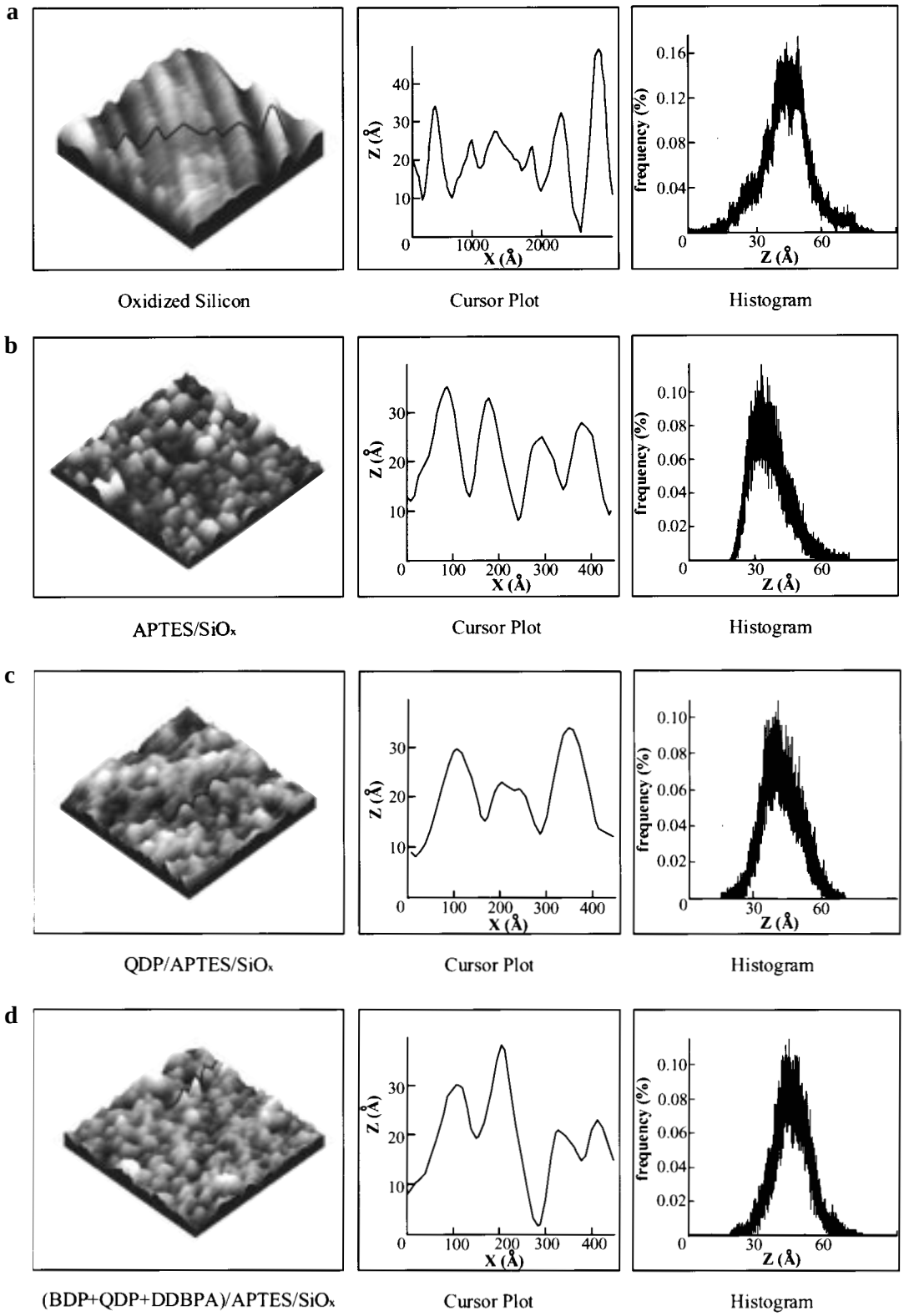

Figure 2. Topographic images (left panels) of the surfaces of (a) oxidized silicon (SiO_x) substrate, (b) APTES-primed substrate, (c) primed substrate with a monolayer of QDP adsorbed, and (d) a mixed monolayer of 5% BDP, 50% QDP, and 45% DDBPA on a primed substrate. The total scanning area is 1000 × 1000 Å except for (a) which is 3000 × 3000 Å. The cantilever force constant is 0.1 N/m, and the imaging force used here is ~0.2 nN. Corresponding cursor profiles and histograms are shown in the middle and right panels, respectively.

narrower distribution in terms of roughness. The typical cluster size is ~130 Å, with an average nearest neighbor separation of ~200 Å. A large number of small clusters 40−100 Å in diameter are present in the mixed layer of 5% BDP, 50% QDP, and 45% DDBPA, and for this monolayer, the typical inter-cluster separation is ~130 Å. Because of the change in surface morphology associated with the formation of chromophore layers, we conclude that aggregates form coincident with the growth of these layers. The growth of chromophore layer is thus not simply a decoration of the primed substrate, but aggregation among chromophore molecules also plays an important role.

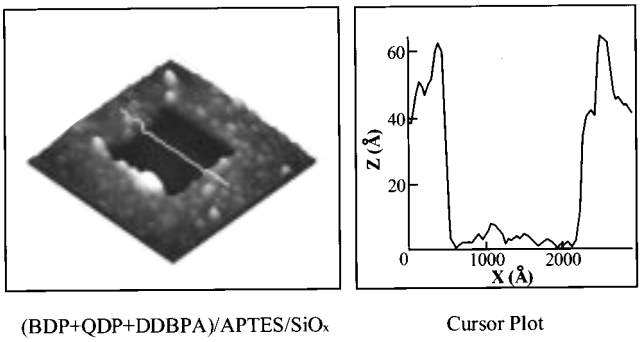

Figure 3. Topographic image of a mixed monolayer of 5% BDP, 50% QDP, and 45% DDBPA on a primed substrate. The molecules in the central 2000 × 2000 Å area were displaced prior to this image using an AFM tip under a force of 1 nN. The overall scanning area is 4000 × 4000 Å acquired at a reduced imaging force of 0.05 nN. The cursor profile reveals the thickness of the layer to be 40 ± 10 Å.

As pointed out earlier, the sizes of most of the aggregates are on the order of hundreds of angstroms. For our sample preparation conditions, we do not see formation of bulkier aggregates or thicker films. The thickness of each film was measured using optical null ellipsometry. A typical thickness for the three-component mixed layer is 40 ± 10 Å, with the uncertainty mainly attributed to the roughness of the substrate and the aggregates. This ellipsometric thickness is verified by AFM measurements (Figure 3). QDP films exhibit the same thickness as the mixed layer, as measured by AFM. The AFM data provide a sound physical picture of monolayer morphology. The next step in this work is to understand the transient optical response of these monolayers and establish how that response is related to their morphology.

Optical Spectroscopy. To appreciate the structural information content of the lifetime data, it is important to consider the result one would recover for a uniform monolayer. The systems we report on here, specifically, mixed BDP and DDBPA monolayers, mixed QDP and DDBPA monolayers, and mixed BDP, QDP, and DDBPA monolayers on oxidized Si(100), all yielded the same nonexponential excited-state population relaxation decay (Figure 4). The regressed time constants for these data are independent of chromophore concentration. This is an expected result, as we discuss below.

In a monolayer where each of the constituents is distributed statistically, the average distance between a donor and the nearest acceptor depends sensitively on the concentration of each. The Förster model predicts that the rate constant for excitation transfer, and therefore, the donor radiative lifetime depends inversely on the D−A spacing to the sixth power (eq 1).[36,37]

$$k_{D-A} = \frac{3\kappa^2 {R_0}^6}{2\tau_D R^6}$$

$$\kappa = \sin\theta_D \sin\theta_A \cos\phi - 2\cos\theta_D \cos\theta_A \qquad (1)$$

where k_{D-A} is the rate constant for donor−acceptor transfer, κ^2 is a geometric factor to account for the projection of the donor transition moment onto the acceptor transition moment, τ_D is the donor lifetime in the absence of acceptor, R is the D−A distance, and R_0 is the critical transfer radius. This latter term contains information on the spectral overlap between the donor and acceptor and the cross sections of the relevant transitions. There should be a marked acceptor concentration (i.e., R) dependence in the donor lifetime ($k_{D-A}{}^{-1}$) data. We present the

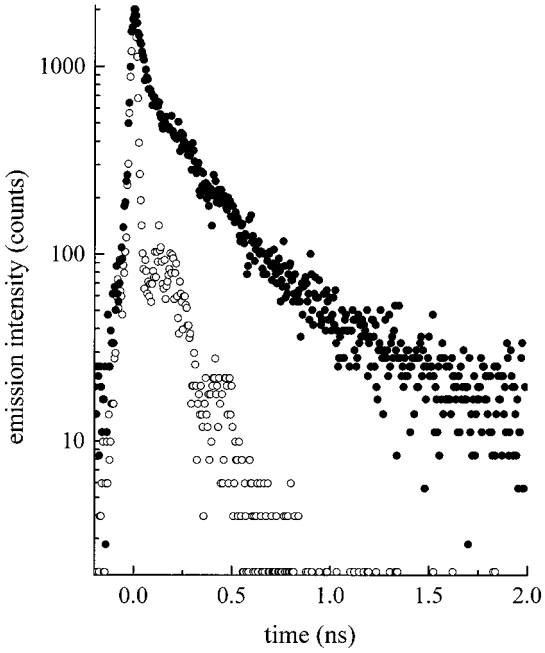

Figure 4. Representative instrument response function (○) and excited-state population decay for QDP in a monolayer (5%) (●).

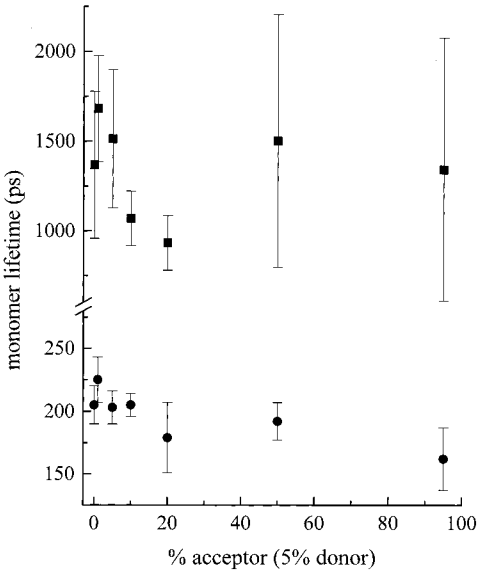

Figure 5. Dependence of donor BDP lifetimes on acceptor QDP concentration, for a monolayer containing 5% donor.

acceptor concentration dependence of the donor lifetimes for the mixed BDP and QDP system in Figure 5. There is no discernible acceptor concentration dependence on the donor lifetimes.

The apparent absence of energy transfer is a consequence of the morphology of the monolayers. An underlying assumption of the Förster model is the homogeneity of the monolayers and that the chromophores behave as individual entities. We know from the AFM data that this assumption must be at least suspect. We consider a model of excitation transport that takes into account a heterogeneous chromophore distribution and aggregation of the chromophores. We want to make clear that the interpretation of the spectroscopic data that follows necessarily contains approximations because of our inability to determine certain system parameters. The discussion is meant to provide an estimate, based on our best guesses for the relevant quantities, of the physical properties of the monolayers. We do not rely

Table 1. Fits of Excited-State Lifetime Data and Simulated Lifetime Data to the Function $f(t) = A_1 \exp(-t/\tau_1) + A_2 \exp(-t/\tau_2)$

	τ_1 (ps)	τ_2 (ps)
BDP on silicon	187 ± 11	1140 ± 377
QDP on silicon	228 ± 45	1254 ± 152
simulated data	197	1230

Scheme 2. Kinetic Model for Population Decay Dynamics in the Monolayers[a]

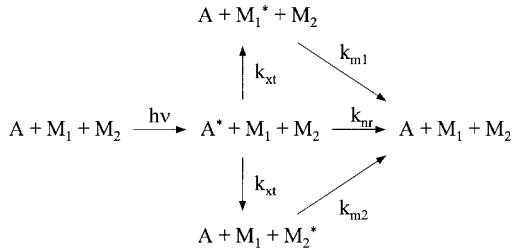

[a] A refers to the aggregate species, and M_1 and M_2 are monomers in different chemical environments.

on the results of the excitation transport calculations to make firm conclusions about interface morphology. Rather, it is the close correspondence between the model predictions and actual AFM data that is of interest.

The functionality of the population decays of the individual chromophores reflects the "spectroscopic" morphology of the monolayer. Previously, we reported the presence of two lifetime components for oligothiophene-containing monolayers, in contrast to the single-exponential decay found for these same chromophores in dilute solution. We recover the same time constants within the uncertainty of our measurements for both BDP and QDP (Table 1), and these lifetimes are invariant with respect to their concentrations in the monolayer or the emission wavelength collected. These results are reminiscent of those seen for the population relaxation of a stilbazolium dye in a Langmuir−Blodgett film.[30] In that work, it was found that the chromophores aggregated significantly and the majority of the radiative decay originated from monomer species that were present in more than one environment.

In a chromophore aggregate, the molecules are spaced closely, (we take this spacing to be ∼5 Å for the ZP lattice) so excitation transport can compete effectively with radiative decay. As a consequence, aggregates are typically characterized by a fluorescence quantum yield significantly lower than that of the corresponding monomer. The dominant emissive response of such a system is considered to be from the remaining nonaggregated, free monomers. The proximity of radiative monomer chromophores to the aggregates can, of course, vary widely, but we consider the two most likely cases for our conditions. Either the monomer is present as a structural defect within an aggregate or it exists near the perimeter of an aggregate. The dielectric response of these two environments will differ significantly, and we thus expect the two types of monomer to be characterized by different lifetimes.[38,39]

Song et al. have developed a model to describe the excitation dynamics of H-aggregates of stilbazolium dyes in Langmuir−Blodgett layers.[30] In this model, depicted in Scheme 2, an aggregated island of chromophore molecules, A, is excited by a short pulse of light. The excitation can decay radiatively (a low probability event), or it can execute diffusive excitation transport ("hopping") about the island until it reaches a radiative monomer. The radiative monomer could be located within the island (M_1) or in the interisland interstices (M_2). A series of coupled differential equations describes the temporal evolution

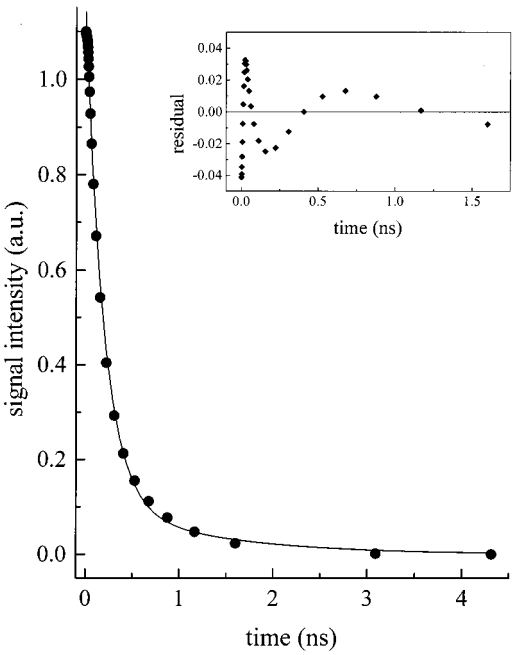

Figure 6. Simulated population decay (●) using eqs 2 (see text) and fit of data (—) to a double-exponential decay function of the form $f(t) = A_1 \exp(-t/\tau_1) + A_2 \exp(-t/\tau_2)$. Inset is a plot of the residuals of the fit.

of monomer and aggregate populations as given in Scheme 2. These equations can be solved numerically to yield the time course of the populations of M_1 and M_2.

$$\frac{d[A^*]}{dt} = -k_{xt}[A^*]([M_1] + [M_2]) - k_{nr}[A^*]$$

$$\frac{d[M_1^*]}{dt} = -k_{M_1}[M_1^*] + k_{xt}[A^*][M_1]$$

$$\frac{d[M_2^*]}{dt} = -k_{M_2}[M_2^*] + k_{xt}[A^*][M_2]$$

$$\frac{d[M_1]}{dt} = k_{M_1}[M_1^*] - k_{xt}[A^*][M_1]$$

$$\frac{d[M_2]}{dt} = k_{M_2}[M_2^*] - k_{xt}[A^*][M_2] \qquad (2)$$

In the numerical simulations, we assume that the aggregates are excited initially, with the populations of excited monomers being established by excitation migration. We estimate $k_{xt} = 10^{13}\ s^{-1}$, a value consistent with excitation hopping in LB films of stilbazolium dyes. We can place limits on this value, as we discuss below. We estimate, on the basis of the conservative assumption that $\phi_{fl} = 0.10$ for aggregated BDP and $\tau_{fl} = 200$ ps for BDP monomer in solution, that the nonradiative decay rate constant $k_{nr} = 4.5 \times 10^8\ s^{-1}$ for the aggregates. While the actual value of k_{nr} may differ somewhat from this estimate, its value does not affect the results of the simulation significantly because k_{nr} is orders of magnitude smaller than k_{xt}. The lifetimes of M_1 and M_2 were varied to produce a decay that closely approximates the experimental population decays. The values used in this simulation (Figure 6) were $k_{M_1} = 7.0 \times 10^9\ s^{-1}$ ($\tau_{M1} = 197$ ps by fitting) and $k_{M_2} = 1.6 \times 10^9$ ($\tau_{M_2} = 1230$ ps by fitting). The simulated curve can be fit to a double-exponential decay even though four rate constants are used to

construct it. While the double-exponential fit does not ostensibly account for the dynamics of the chromophores in the monolayer, it provides a useful empirical representation of the relaxation phenomena we measure with the TCSPC experiment. Regression of the experimental data using a double-exponential function produces residuals that match those shown for the fit to the model in Figure 6.

Two model parameters are related to the aggregate size sensed by the lifetime measurement. These are k_{xt} and the number of excitation transport events, n, required for the aggregate-supported excitation to find a monomer and decay radiatively. The total hopping time ($k_{xt}^{-1}n$) can be related to average distance traveled by means of a Monte Carlo simulation, as has been reported before.[30] The results of the Monte Carlo simulation do not depend on the specific chemical system under investigation. The results of the simulation depend on the physical properties of the system and on Brownian statistics. The experimental manifestation of the migration of an excitation to a radiative monomer will be a build-up in our single photon counting signal after time zero. Despite the fact that our instrument response function is short (∼30 ps), it is longer than the expected build-up time and we do not resolve a build-up directly. In an attempt to determine whether there is a build-up in the experimental fluorescence intensity data at early times, we have attempted deconvolution of the response function from the monolayer signal. While we do see a build-up in the deconvoluted data, the actual time constant we recover for the build-up depends sensitively on the initial parameters used in the deconvolution procedure. We therefore do not report an explicit value for this build-up time. Rather, we place an upper bound of 10 ps on the excitation migration time ($k_{xt}^{-1}n \leq 10$ ps). We can thus place a corresponding upper bound on the size of the aggregate island(s) sensed by the measurement.

The correspondence between our spectroscopic data and the physical size of the aggregates is, of course, limited by the accuracy of our approximations. We consider two limiting cases of aggregate-to-monomer transfer because this step can, in principle, affect the estimate of island size. In the first case, the radiative monomers are close in proximity to an island, perhaps even within the island but residing in a physical position that precludes their participation in the aggregate structure. In this case, the last transfer event, from the aggregate to the monomer, is fast. As detailed above, we cannot quantitate the lifetime of the aggregate excitation, so we use the upper bound value of $\tau_{xt} \approx 10$ ps. The time constant per excitation transfer event, or hop, is taken to be 0.1 ps, so in 10 ps, an average of 100 hops can occur. Song et al. have published the results of calculations where the dynamics of exciton motion within an H-aggregate were modeled using a random walk approach.[30] This calculation produces a curvilinear relationship ($n^{1/2}$) between mean distance traveled for exciton diffusion and the number of steps taken. For 100 hops, the mean distance traveled is 40 Å. With an approximate 5 Å spacing between lattice sites in the zirconium−phosphonate lattice, the exciton can travel ∼8 lattice separations within the aggregate. The actual aggregate shape will, of course, play an important role in determining the island size in this model, and it is clear that the results will depend on the aspect ratio of the island. The simplest case for this calculation is a square island, for which we obtain an average aggregate size of 64 molecules.

In the second limiting case, where the radiative monomer is not in direct contact with the aggregate, the last transfer step will not be as efficient, consistent with the Förster R^{-6} dependence (eq 1). We calculate the critical transfer radius, $R_0 = 57$ Å for the BDP/QDP system.[22] Using this critical radius, a radiative lifetime of $\tau_{rad} = 200$ ps and $\tau_{xt} = k_{D-A}^{-1} = 0.1$ ps, the maximum D−A spacing is calculated to be $R = d_{max} = 16.3$ Å.[37] In the simplest model of the surface, where all the aggregates are spaced evenly, $d_{max} \sim 2.15\sqrt{N}$. Thus $N = 57$ molecules, in essentially exact agreement with the first case. The location of the radiative monomers relative to the aggregate is thus not a deterministic factor in the spectroscopic estimation of the aggregate size.

Realistically, the model predicts "spectroscopic" aggregates of 50−100 molecules in size. For a 5 Å intersite spacing and a square aggregate, we estimate the aggregate size to be on the order of 50 × 50 Å. It is reasonable to expect that the density and type of defects within the aggregates will determine the "spectroscopic size". There is no fundamental reason, however, why the physical aggregate size determined from AFM measurements must be in close agreement with the spectroscopic size we have determined. The fact that there is excellent agreement between the two measurements suggests significant organization within the aggregates.

Roles of Priming Chemistry and Substrate in Determining Monolayer Morphology. Because the morphology of these layered interfaces depends on both the priming and adsorption chemistries, it is important to understand the reason(s) for the formation of the three-dimensional islands in the first place. In an earlier paper we reported on the surface relief characteristics of the substrates.[41] That roughness, while important to the motional properties of the chromophores, does not address the basis for the island formation seen in this work.

There are at least three factors contributing to the formation of the islands. The dominant ones are the intrinsic surface roughness and the apparently heterogeneous distribution of active silanol groups on the substrate,[41−44] the nature of the priming chemistry used to form aggregated structures, and the ability of the chromophores to aggregate either before or during the layer formation process.

In an ideal experiment, we could control selected surface properties independent of one another by using different materials. Unfortunately, this level of control is not achievable in materials as complex as silicon oxides. Comparison of mica and SiO_x substrates involves changes in both surface roughness and silanol group density, and it is not possible to fully decouple these surface properties. Nonetheless, it is instructive to examine the consequences of the priming chemistry on these two surfaces. We have imaged APTES on mica(001), an atomically flat surface known to possess relatively few hydroxyl groups. The surface of APTES/mica, with a thickness of 7 ± 3 Å as measured by AFM, is much more homogeneous than an APTES/SiO_x surface. In addition, the force required to displace APTES on mica is not as high as it is for APTES on SiO_x, indicating the importance of surface silanol group density. On the mica surface, scattered three-dimensional clusters are seen due to the lower density of silanol anchor sites, where on the APTES/SiO_x surface, relatively dense three-dimensional aggregate structure is characteristic (Figure 2).

The primer layer chemistry determines both the stability and the morphology of the primer layer. These properties, in turn, determine the growth behavior of subsequent layers. Priming a SiO_x or oxidized Si surface with APTES is known to produce a cross-linked structure because of the three reactive function-

(42) Wang, H.; Harris, J. M. *J. Phys. Chem.* **1995**, *99*, 16999.
(43) Lochmuller, C. H.; Colborn, A. S.; Hunnicutt, M. L.; Harris, J. M. *J. Am. Chem. Soc.* **1984**, *106*, 4077.
(44) Lochmuller, C. H.; Colborn, A. S.; Hunnicutt, M. L.; Harris, J. M. *Anal. Chem.* **1983**, *55*, 1344.

alities present on each primer molecule.[45] In an effort to address the role of the Si−O cross-linking, we have also made monolayers using APDMES. For this primer there is only one ethoxy group per molecule to react with the substrate, eliminating the possibility of cross-linking. Using this chemistry, we observe more homogeneous surface. The non-cross-linked APDMES priming layer is not as stable as the polymerized APTES layer. APDMES can be displaced with 0.1 nN of imaging force, and greater than 1 nN is required to displace APTES. Of key importance is that, when a chromophore monolayer is formed on the APDMES-primed substrate, we observe spectroscopic population relaxation dynamics identical to those seen for an APTES-primed monolayer. Aggregates are seen spectroscopically even for monolayers where the potentially complicating role of the priming chemistry has been precluded, providing direct evidence for the importance of chromophore aggregation during the layer formation process.

Conclusion

The combination of AFM and excited-state population decay measurements has afforded substantial insight into the mesoscopic morphology and molecular-scale organization of zirconium−phosphonate monolayers used in this and previous studies.[31,41] The presence of aggregate islands accounts for the functionality of our transient population decay behavior. The size and separation of the islands, as resolved by AFM, reveals a clear correspondence between physical and spectroscopic measurements of the interface. The origin of the island structures in the primer layer of these assemblies appears to lie with the heterogeneous distribution of the active silanol sites on the substrate. The aggregates formed by the chromophores derive their characteristic sizes from both the features of the primer layer and their own propensity for aggregation, either before or during the adsorption process. These findings will be important in evaluating interlayer excitation transport effects in more complex multilayer structures.

Acknowledgment. We are grateful to the National Science Foundation for support of this work through Grant CHE 95-08763 (G.J.B.). G.Y.L. wishes to thank Arnold and Mabel Beckman Foundation for a Young Investigator award. J.C.H. acknowledges support from a James L. Dye Endowed Fellowship.

JA982182R

(45) Haller, I. *J. Am. Chem. Soc.* **1978**, *100*, 8050.